Invitroefficacy Of Poly-Gama-Glutamic Acid Loaded Nano-Formulation Of Levofloxacin Against Brucellosis.

Arijit Shil[1*], Prof.(Dr.) Paramita Dey[2], Dr. Tapan Kumar Mondal[3]

[1*]Faculty, Department of Diploma in Veterinary Pharmacy, West Bengal University of Animal and Fishery Sciences, Government of West Bengal. Mohanpur Campus, Nadia, West Bengal, India.
[2]Professor, Department of Pharmaceutics, Bengal School of Technology, A College of Pharmacy, Chinsurah, Hooghly, West Bengal, India
[3]Former Vice –Chancellor West Bengal University of Animal and Fishery Sciences, Government of West Bengal, India

Abstract

Levofloxacin and Moxifloxacin are indeed a fluoroquinolone antibiotic that can be used in the treatment of brucellosis, which is caused by the bacteria of the Brucella genus. It is often used in combination with other antibiotics to treat this infection effectively. The choice of antibiotics for treating brucellosis can vary depending on factors such as the specific Brucella species causing the infection, the patient's overall health, and any antibiotic resistance patterns in the region. Levofloxacin and Moxifloxacin are one of the antibiotics that can be considered for the treatment of brucellosis, but the treatment plan should be determined by a healthcare provider who can tailor it to the individual patient's needs. In this research work, levofloxacin(LEV) and Moxifloxacin (MOX) were prepared by using of poly (gama glutamic acid) (PGA) and Polyviny alcohol (PVA) nanoparticles with the purpose of targeting drug delivery system against brucella. A thorough study has been carried out in order to optimize the preparation of LEV, Mox-loaded polymeric nanoparticles (NPs) suitable for Brucella bacterial treatment. Changes in the preparation method, in the organic solvent nature, in the pH of the aqueous phase, or in the temperature were investigated. The physical and chemical analysis of the nanoparticles (NPs), as well as their encapsulation efficiency (EE) and the controlled release of LEV in a laboratory setting, indicated that the most effective formulation was achieved through the emulsion-solvent evaporation method utilizing dichloromethane as the organic solvent. This resulted in the production of well-suited PLGA NPs loaded with LEV. The morphology of these NPs was investigated using SEM. Their antimicrobial activities against brucella microorganisms were determined in vitro measuring the minimum inhibitory concentration (MIC). The results show that the use of these loaded LEV, MOX, PGA nanoparticles has the advantage of the slow target drug release of the antibiotic, which would permit an increase in the time period between administrations as well as to decrease the side effects of the drug.

Keywords: *Levofloxacin, Moxifloxacin, Nanoparticles, Targeted drug delivery system, Brucella treatment*

1. INTRODUCTION:

Brucellosis is a zoonotic infection caused by bacteria of the genus *Brucella*. It primarily affects animals but can also be transmitted to humans, typically through contact with infected animals or consumption of contaminated animal products (1). The disease has a global distribution and is particularly prevalent in regions where livestock farming is common and preventive measures are less rigorous. The bacteria responsible for brucellosis are small, gram-negative, facultatively intracellular coccobacilli (2). The primary species of *Brucella* that cause infection in humans are:

a. *Brucella melitensis*: Primarily affects sheep and goats and is the most virulent species for humans.
b. *Brucella abortus*: Mainly infects cattle and is the most common cause of brucellosis in humans.
c. *Brucella suis*: Affects pigs and occasionally causes human infections.
d. *Brucella canis*: Affects dogs and can also infect humans but is less common.

Fig 1: Zoonotic Brucella Bacteria

1.1 Transmission:

The most common route of transmission to humans is through direct contact with infected animals or ingestion of contaminated animal products, particularly unpasteurized dairy products such as milk, cheese, and cream. In rare cases, *Brucella* can be transmitted through inhalation of aerosols containing the bacteria, a risk primarily for veterinarians, farmers, and laboratory workers. Transmission between humans is extremely rare but can occur through sexual contact or blood transfusion (3).

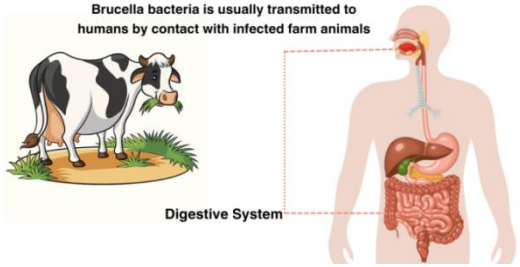

Fig 2: **Transmission of Brucella Bacteria; animal to human**

1.1.1 Pathogenesis:

Once *Brucella* enters the body, it is phagocytosed by macrophages but survives and replicates within these cells (4). The bacteria evade the immune response by preventing the fusion of phagosomes with lysosomes, allowing them to persist in the reticuloendothelial system (such as the liver, spleen, and lymph nodes).

The infection can lead to chronic granulomatous inflammation, and untreated or inadequately treated cases may result in long-term complications. *Brucella* has a predilection for organs rich in reticuloendothelial tissue, such as the liver, spleen, and bone marrow (5). Brucellosis presents with a wide variety of clinical symptoms, making it challenging to diagnose. Symptoms may range from mild to severe and can be acute, subacute, or chronic, depending on the duration and severity of the infection.

Treatment:

Treatment of brucellosis involves the use of specific antibiotics aimed at eliminating the bacteria and preventing relapses. Because *Brucella* bacteria can persist inside host cells, long-term combination antibiotic therapy is typically required to ensure effectiveness and to prevent chronic or recurrent infections (8). The treatment of brucellosis involves a combination of antibiotics to ensure that the bacteria are eradicated from both extracellular and intracellular compartments. Doxycycline (100 mg twice daily for 6 weeks) combined with rifampicin (600-900 mg daily for 6 weeks)**.** Alternative regimens may include streptomycin or gentamicin in combination with doxycycline, particularly for severe cases or where complications such as neuro brucellosis are present. Treatment failure and relapses can occur, often due to inadequate treatment duration, poor drug penetration into infected tissues, or failure to adhere to the treatment regimen (9).

Activity of Fluoroquinolones Against Brucella Bacteria:

Fluoroquinolones are a class of antibiotics with broad-spectrum activity that have shown effectiveness in treating Brucella infections (brucellosis), though they are not typically the first-line treatment. Their use in the management of brucellosis has been explored, particularly in cases of resistance to standard treatments or when conventional therapy is contraindicated (7). Fluoroquinolones work by inhibiting bacterial DNA gyrase and topoisomerase IV, enzymes essential for bacterial DNA replication, transcription, and repair. This mechanism leads to the death of the bacterial cell. In the case of Brucella bacteria, fluoroquinolones can penetrate intracellular environments, which is crucial for treating intracellular pathogens like Brucella that survive and replicate inside macrophages (8).

Use of Fluoroquinolones against Brucellosis:

Fluoroquinolones, such as ciprofloxacin and ofloxacin, have been studied as part of combination therapy for brucellosis. They are often used in combination with rifampin or doxycycline. The rationale for combination therapy is to reduce the risk of relapse, which is common with single-drug regimens. Ciprofloxacin has demonstrated moderate efficacy in treating acute brucellosis. However, when used as monotherapy, there have been concerns about high relapse rates (10). For this reason, fluoroquinolones are usually combined with other antibiotics, such as doxycycline or rifampin, to improve treatment outcomes. One of the advantages of fluoroquinolones in brucellosis treatment is their ability to penetrate intracellular environments. Brucella species are intracellular pathogens that survive within macrophages (8). Fluoroquinolones' ability to reach intracellular concentrations and kill the bacteria within macrophages makes them a useful option, especially in combination with other drugs that also target intracellular organisms. Relapse is a common challenge in brucellosis treatment, particularly in cases of chronic brucellosis or when patients have not completed their antibiotic regimen. Studies have shown that fluoroquinolones, particularly ciprofloxacin, can be beneficial in treating relapsed cases when used in combination with rifampin or doxycycline (9, 4).

Nano-particles:
Nano-particles, defined as particles with dimensions less than 100 nanometers, have garnered substantial interest across various scientific disciplines due to their unique properties, such as high surface area-to-volume ratio, quantum effects, and enhanced reactivity. These distinct characteristics emerge at the nano-scale, differing significantly from their bulk counterparts, thereby enabling novel applications in fields such as medicine, electronics, energy, and materials science. The development and study of nanoparticles have opened up new frontiers in nanotechnology, offering solutions for drug delivery systems, targeted cancer therapy, and the creation of more efficient catalysts in chemical reactions. (10, 9). Nanoparticles can be classified into several categories based on their composition and properties, including metallic, polymeric, ceramic, and semiconductor nanoparticles. Each type exhibits specific attributes suitable for various applications.

Nanoparticles in Targeted Drug Delivery Systems:
Targeted drug delivery using nanoparticles has emerged as a powerful and innovative approach in modern medicine, aiming to enhance the therapeutic efficacy of drugs while minimizing systemic toxicity (11). Nanoparticles offer a unique platform for delivering drugs precisely to the disease site, especially in conditions such as cancer, cardiovascular diseases, and infectious diseases. By modifying the surface of nanoparticles and loading them with therapeutic agents, nanoparticles enable controlled and targeted drug delivery, leading to improved pharmacokinetics, biodistribution, and therapeutic outcomes (12). The concept of targeted drug delivery revolves around the ability to direct therapeutic agents specifically to diseased tissues or cells while minimizing exposure to healthy cells. Traditional drug delivery systems often suffer from non-specific distribution throughout the body, leading to off-target effects and limited therapeutic efficiency (13). Mechanisms of Targeting in Nanoparticle-Based Drug Delivery:

MATERIALS AND METHODS

MATERIALS

The successful formulation and development of a dosage form depend on the precise selection of active pharmaceutical ingredients and excipients that are compatible within the medicinal product. In this study, PGA was employed as the foundational polymer for the preparation of polymeric nanoparticles. Alongside the polymer, a comprehensive list of chemicals, reagents, and active pharmaceutical ingredients utilized in the formulation is provided below. Additionally, detailed information on these materials has been included in the below for reference in future work.

CHEMICAL MATERIALS AND POLYMERS

Materials used in present investigation

Chemical Name	Grade	Source
Levofloxacin	IP	Macleods Pharma, Sikkim
Moxifloxacin	IP	Macleods Pharma, Sikkim
Poly gama glutamic acid	IP	Shimzu Biotech, China
Ethyl acetate	LR	Shimzu Biotech, China
Tween 80	LR	Shimzu Biotech, China

Table 1: Detail information about chemicals

5.2.2 CHEMICAL REAGENTS AND OTHERS SOLVENTS

List of Chemicals and Reagents

Chemical Name	Grade	Source
Methanol	LR	WBUAFS,NADIA
Alcohol	LR	WBUAFS, NADIA

Table 2: Detail information about chemicals reagents

METHODS :

Preformulation study since the study was aimed to develop a polymeric nanosize dosage form, therefore the preformulation studies which are associated with formulation parameters of polymeric nanoparticles were only performed in the present study.

Physical appearance of the drug: The obtained drug sample was examined visually, using a microscope, and against both black and white backgrounds to assess its physical properties and color. The observations were then compared with the details provided in official reference sources.

Melting point: A small portion of the obtained drug sample was placed into a capillary tube with one end sealed. The tube was securely attached to a calibrated thermometer and heated in a Thiele's tube. The temperature range during which the sample melted was recorded and then compared with the melting point reported in the literature.

UV-Visible absorption:

Levofloxacin, weighing 10 mg, was dissolved in 5 ml of methanol, and the solution was diluted with distilled water to a final volume of 100 ml. From this, 1 ml of the solution was further diluted with water to 10 ml to obtain a 10 µg/ml

methanolic solution of levofloxacin. This solution was scanned between 200 and 400 nm using a UV-Visible spectrophotometer to obtain the absorption spectrum. The λmax value was recorded and compared with the value reported in the literature (16).

Organic Solvent Screening

The solubility of levofloxacin was assessed using the phase-solubility method developed by Higuchi and Connors . In this experiment, four different organic solvents and solvent mixtures were employed. Levofloxacin was incrementally added to the organic phase (1 ml) under continuous vortexing, until saturation solubility was reached. Once saturated, the solution was incubated at 37°C with periodic agitation for 2 hours to achieve complete equilibrium, followed by membrane filtration. The filtered solution was subsequently analyzed to quantify levofloxacin using a validated LC-MS/MS method.

Effective solvent screening is essential for ensuring the solubility of all formulation components. Solubility testing is a standard procedure for solvent selection during formulation development. In this study, both levofloxacin and PGA needed to be dissolved in the selected solvent, as the solubility of PGA is critical for establishing a stable emulsion. To evaluate PGA solubility, an excess of PGA (100 mg) was accurately weighed and placed into a 2 ml Eppendorf tube. The selected solvents were then added, and the mixture was vortexed for 10 minutes. Following vortexing, the samples were allowed to stand for 30 minutes to allow undissolved polymer to sediment (17).

Evaluation of Physicochemical Properties

Fourier Transform Infrared (FTIR) Analysis

The chemical stability and interaction between the PGA, drug, and excipients (such as PGA) in the nanoparticles (NPs) were evaluated by detecting the characteristic bond vibrations of each component using FTIR spectroscopy (Model: Nicolet iS10, Thermo Fisher Scientific, USA). For this analysis, the samples were scanned across a wavelength range of 400 to 4000 cm^{-1}. This method helps to ensure the chemical integrity of the components in the NPs.

Differential Scanning Calorimetry (DSC)

The physical integrity of the drug and excipients was assessed by measuring the temperature at which heat exchange occurs during the physical transformation of the compounds. Each component of the formulation has a specific identification value, such as the glass transition temperature for amorphous substances and the melting point for crystalline materials, which should remain unchanged after the preparation of nanoparticles (NPs). To detect any alterations in these characteristics, individual samples of the active pharmaceutical ingredient (API) and excipients (PGA, PVA) were analyzed, along with a physical mixture of all components, to ascertain their melting point and glass transition temperature. The differential scanning calorimetry (DSC) study was conducted in a controlled inert atmosphere, with a heating rate of 10°C/min over a temperature range of 5°C to 350°C, maintained under a constant nitrogen flow of 40 ml/min (14).

X-ray Diffraction (XRD) Analysis

X-ray diffraction (XRD) analysis provides insights into the crystallinity of samples, thereby aiding in the identification of the physical characteristics of the compounds. The properties of the pure drug, PGA, blank nanoparticles, and drug-loaded nanoparticles were assessed using the Ultima III X-ray diffractometer (Rigaku), equipped with a copper-targeted K-beta filter. For the analysis, powdered samples were placed on a quartz plate and smoothed to achieve a flat surface. The XRD patterns were recorded over a diffraction angle range of 5 to 90 degrees (2θ) with a step size of 0.05 degrees and a scanning speed of 3°/min

Surface Morphology Analysis

The surface characteristics of the drug and excipients were examined using scanning electron microscopy (SEM) with the EVO 18 model (Special Edition, ZEISS). Dried samples were carefully mounted on stubs using carbon adhesive. To enhance conductivity, the samples underwent two rounds of platinum sputtering using a mini coater (Quorum Q150T ES). The morphology was then assessed directly under the SEM at two distinct magnification levels: 10,000X and 20,000X.

RESULT AND DISCUSSION:

Before progressing to the nanoformulation stage, a thorough pre-formulation evaluation was performed. This involved an in-depth examination of the physicochemical characteristics of the drugs and excipients to ensure product stability and enhance therapeutic effectiveness. In this research, nanoparticles were prepared using the double emulsion solvent evaporation technique. A key focus was placed on understanding the essential processes that contribute to the formation of a stable emulsion and the successful encapsulation of the drug within the polymer matrix. To meet the study's goals, essential pre-formulation tests were conducted, including the choice of organic solvents, solubility analysis, crystallinity, FTIR, and DSC evaluations (18).

Determination of organic solvent and solubility

Nano-emulsions are biphasic liquid systems consisting of oil and water phases. The development of polymeric nanoparticles using the double emulsion solvent evaporation method, which stabilizes both phases, is a highly intricate process. A key factor in nano-emulsion stability is the solubility of the drug. For the oil phase preparation, a volatile organic solvent is necessary to achieve uniform dissolution of the drug and polymer. Research shows that the choice of organic solvent and the solubility of the drug are crucial in determining how well the drug disperses within the polymer matrix. Ethyl acetate was identified as an effective solvent for both PGA and Levofloxacin but led to crystal formation within the nanoparticles. In contrast, a 5:3 mixture of ethyl acetate and ethanol improved Levofloxacin's solubility and reduced crystal formation. The high melting point and crystalline structure of Levofloxacin present challenges for its solubility in organic solvents, which in turn affects the uniformity of the solid dispersion within the nanoparticles. Therefore, drug solubility played a critical role in solvent selection, which was guided by solubility data. The study found that ethyl acetate and ethanol mixtures in 8:2 and 5:3 ratios offered the best solubilizing properties. After multiple trials, the optimal solvent ratio was determined to be 50:30 (ethyl acetate:ethanol), achieving the highest Levofloxacin solubilization. All formulations were prepared using these solvents to evaluate the impact on various parameters, ensuring a thorough assessment (19).

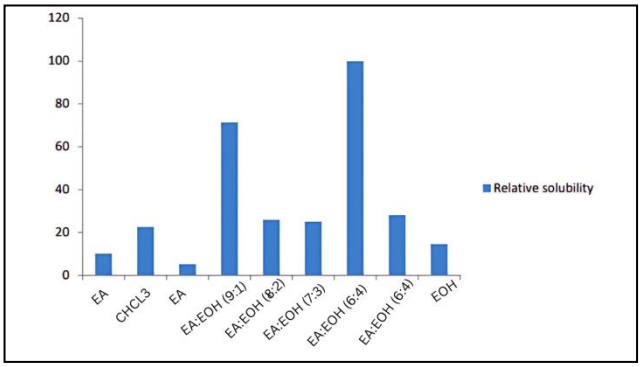

Figure 3: Relative solubility of levofloxacin in different organic solvents.

Determination of Crystallinity

The presence of crystalline active pharmaceutical ingredients (APIs) can greatly affect the distribution of the drug within a polymer matrix, potentially reducing the therapeutic effectiveness of the dosage form. One approach that has gained considerable attention for improving drug dissolution is solid dispersion (SD) using hydrophilic polymers. This method enhances solubility by transforming crystalline drugs into an amorphous state and improving wettability. The degree of crystallinity reflects the amount of crystalline material present in a sample. Drugs with high melting points, such as Levofloxacin, are especially susceptible to crystal formation during formulation and prolonged storage, leading to uneven solid dispersion within nanoparticles (20).

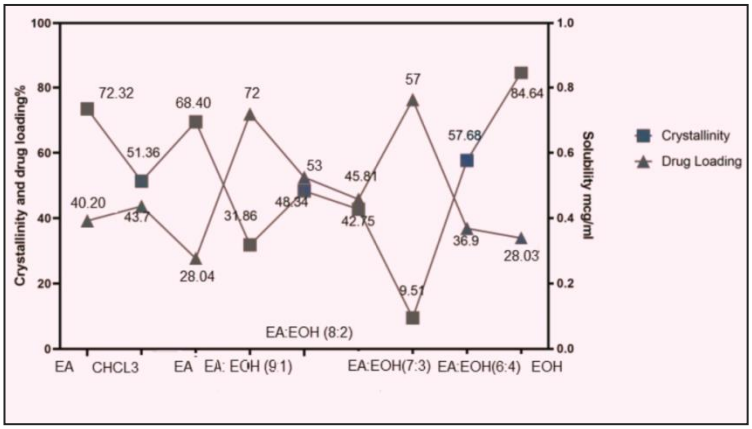

Figure 4: A comparative graphical representation of crystallinity and drug loading.

Solid phase characterization of drug and excipients

FTIR study

The compatibility between the drug and excipients was assessed using Fourier Transform Infrared (FTIR) spectroscopy, analyzing a physical mixture that included all required components. FTIR spectra for Levofloxacin, PGA, and their physical mixture were recorded over the range of 3600 cm^{-1} to 400 cm^{-1}. Levofloxacin exhibited characteristic peaks at 1892.36 cm^{-1}, attributed to aromatic C-H stretching in benzene rings; 1455.40 cm^{-1}, corresponding to aliphatic C-H stretching; 1492.86 cm^{-1}, associated with the carbonyl (C=O) group in carboxylic acids; and 1315.90 cm^{-1}, indicating the C=C bond in aromatic rings. Additionally, a peak at 728.47 cm^{-1} in the fingerprint region was attributed to ring vibrations of 1,2-disubstituted benzene. The PGA spectrum revealed notable peaks at 1916.73 cm^{-1} (C=O stretching of

the carbonyl group), 1841.65 cm^{-1} (C-H stretching in methyl groups), and 1541.01 cm^{-1} and 1452.70 cm^{-1} (C-O stretching vibrations) (130). Less intense peaks were observed at 1048.86 cm^{-1} (O-H stretching due to hydrogen bonding) and 1196.59 cm^{-1} (C-H stretching from alkyl groups).In the FTIR spectrum of the physical mixture, the key bond vibrations of the individual components remained intact, with no new peaks observed. These findings suggest that no significant chemical interactions occurred between the drug and the excipients.

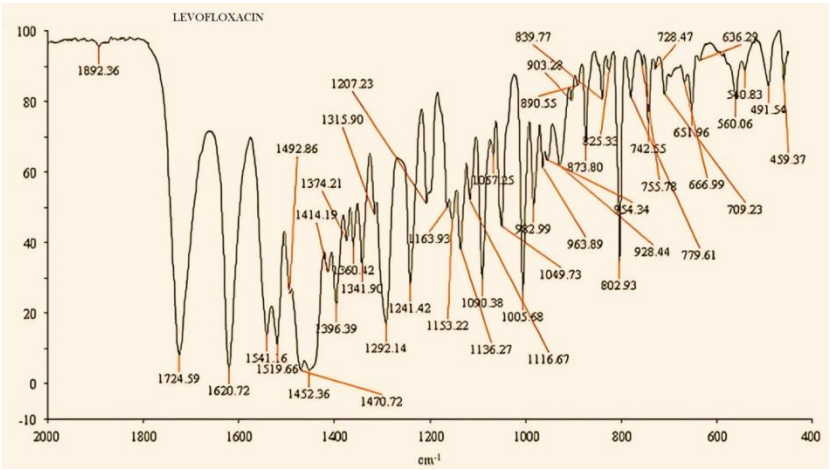

Figure 5: Fourier-transform infrared (FT-IR) spectra of (a) Levofloxacin pure drug

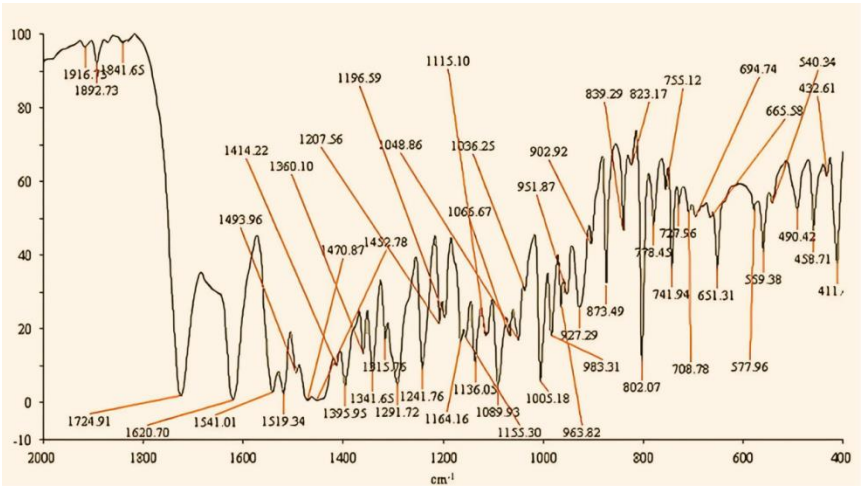

Figure 6: Fourier-transform infrared (FT-IR) spectra of (a) Levofloxacin and Poly (gama glutamic acid) mixture.

XRD study

Determining the physical form of materials is a crucial element in pre-formulation studies, as it can significantly affect the formulation of drug-loaded nanoparticles and their release profiles. To assess the physical properties of the samples, X-ray diffraction (XRD) analysis was performed on the drug, excipient (PGA), and blank nanoparticles. The XRD pattern of pure Levofloxacin displayed distinct diffraction peaks at 6.8°, 14.1°, 15.1°, and 22.2°, confirming its crystalline structure, with the peaks at 6.7°, 14.3°, and 22.3° being particularly prominent. In contrast, the diffractogram of PGA showed a smooth baseline, indicating its amorphous nature. Similarly, the XRD pattern of the blank nanoparticles mirrored that of PGA, demonstrating that no physical transformation of the excipients occurred during the formulation process (19).

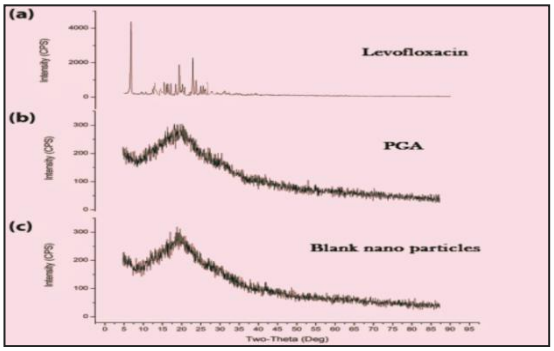

Figure 7 : XRD studies of (a) levofloxacin, (b) PGA and (c) Blank nanoparticles.

DSC study

The thermograms of Levofloxacin, PGA, PVA, and their physical mixture are presented in , offering valuable insights into the thermal properties of these components and helping to identify any potential interactions between the drug and excipients in the solid state. Levofloxacin exhibited a distinct endothermic peak at 278.28°C, which corresponds to its melting point and confirms its crystalline structure. In contrast, PGA showed an endothermic peak at 58.46°C, indicating its glass transition temperature and amorphous nature. The thermogram of the physical mixture displayed the characteristic peaks of the individual components, suggesting that no significant thermal interactions occurred between the drug and the excipients. This confirms the physical stability and compatibility of the components within the formulation (18).

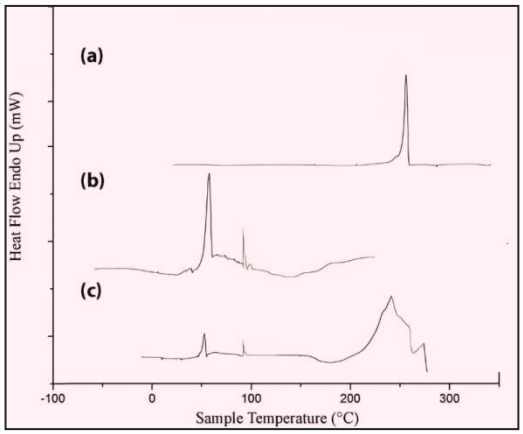

Figure 8 : DSC thermograms analysis of (a) levofloxacin, (b) PGA and (c) Physical mixture.

Morphology of API and polymer

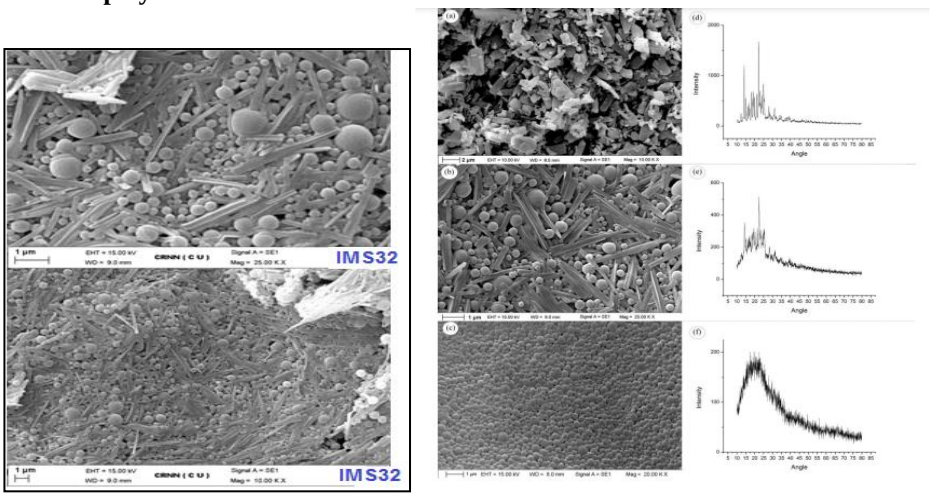

Figure 9: A comparative representation of morphological Formulation

At 10KX magnification, the morphological analysis of pure Levofloxacin (API) revealed a heterogeneous geometric structure with solid particles of varying sizes, indicating a polydisperse distribution . In contrast, the SEM image of the polymer showed macromolecular formations without any defined particle size or shape, further confirming the amorphous nature of PGA .

Formulation technique of polymeric NPs

In this study, a solubility-modulated double emulsion (W/O/W) solvent evaporation technique was employed to develop uniform, spherical drug-loaded polymeric nanoparticles (NPs). This advanced emulsification method facilitates the incorporation of two distinct compartments within a single nanodroplet. The appropriate concentration of polyvinyl alcohol (PVA) as the primary emulsifier stabilized the W/O emulsion, ensuring particle size consistency, which was subsequently reflected in the secondary W/O/W emulsion. High-speed homogenization reduced the primary emulsion droplets to nanoscale, followed by isolation at 27,144g to form W/O/W nanodroplets, resulting in a homogeneous secondary emulsion. To maintain nanodroplet mobility during nanoparticle formation, minimal mechanical stress (340 RPM) was applied (134). The emulsion was magnetically stirred for 12 hours, allowing sufficient time for organic solvent evaporation and solidification of the nanoparticles. A freeze-drying process was then employed to preserve the integrity of the nanoparticles during water removal.

Statistical optimization of nanoformulation

At the outset of development, a comprehensive literature review was conducted to gather essential information on potential variables, methodologies, and control strategies necessary for formulating a product with optimal attributes. This foundational knowledge was critical for addressing formulation challenges and achieving the desired product characteristics.To identify key factors influencing formulation outcomes, potential product and process variables were analyzed using a Plackett-Burman Design (PBD). This approach highlighted significant variables such as PGA content, PVA concentration, and homogenization speed, based on their substantial p-values in the PBD analysis. These insights were then used to refine the formulation process through a Box-Behnken Design (BBD).The independent variables were controlled within narrow ranges to ensure consistency and validate the process. By incorporating three levels of the selected variables, the study demonstrated versatility in predicting central points (5 points) within the BBD framework. This method enabled the development of a scientifically robust model capable of predicting product quality and optimizing conditions for various polymeric nanoparticle applications.

Run	A	B	C	D	E	F	G	H	Particle Size (nm)	Encapsulation efficiency (%)	Zeta Potential
1	1	1	-1	1	1	1	-1	-1	347.3	72	2.2
2	1	-1	1	1	-1	1	1	1	244.1	70	10.7
3	-1	-1	-1	-1	-1	-1	-1	-1	264.7	60	4.2
4	1	1	-1	-1	-1	1	-1	1	340.7	81	2.6
5	1	-1	-1	-1	1	-1	1	1	313.4	74.8	8.3
6	1	1	1	-1	-1	-1	-1	-1	238.2	82.1	10.4
7	-1	1	-1	1	1	-1	1	1	262.7	70.8	8.3
8	-1	1	1	-1	1	1	1	-1	251.9	67.1	9.7
9	-1	-1	-1	1	-1	1	1	-1	328	62.4	10.2
10	1	-1	1	1	1	-1	-1	-1	217.4	74.2	4.8
11	-1	1	1	1	-1	-1	-1	1	238.8	68.1	3.2
12	-1	-1	1	-1	1	1	-1	1	263.4	63.1	2.4

Table 3: Observed responses in Plackett-Burman design.

Response 1: Particle Size					Fit Statistics	
Source	**Sum of squares**	**Mean**	**F-value**	**p-value**		
Model	27624.16	2711.77	182.24	0.000602	Std. Dev.	3.81
PGA Cont.	844.14	844.14	58.30	0.00471	Mean	276.42
PVA %	211.51	211.51	13.40	0.032071	C.V. %	1.34
Hz Speed (rpm)	13130.14	13130.14	894.72	8.18E-04	R^2	0.98
Hz duration	94.74	94.74	6.19	0.08402	Adjusted R^2	0.98
PVA Mw (kDa)	4979.84	4979.82	337.40	0.00033	Predicted R^2	0.94
PGA T-Group	74.50	74.50	5.13	0.108624	Adeq. Prec.	38.72
Residual	44.22	14.72				
Cor Total	47076.51	48				

Note: Hz-Homogenization, Mw-Molecular weight, T-group- Terminal group, Adj-Adjusted, Pred-Predicted, Adeq-Adequate, Prec- Precision .

Table 4: Experimental matrix of PBD (Particle size).

Response 2: Encapsulation Efficiency					**Fit Statistics**	
Source	**Sum of squares**	**Mean**	**F-value**	**p-value**		
Model	570.72	71.72	83.25	0.00028	Std. Dev.	1.083
PGA Cont.	366.40	366.40	357.34	0.0037	Mean	76.45
PVA %	110.52	110.52	94.41	0.0027	C.V. %	1.38
Hz Speed (rpm)	16.28	16.28	14.70	0.029475	R^2	0.99
Hz duration	16.28	16.28	14.49	0.02945	Adjusted R^2	0.98
PVA Mw (kDa)	6.14	6.14	8.45	0.1003	Predicted R^2	0.91
PGA T-Group	8.002	8.002	7.12	0.080	Adeq. Prec.	28.31
Residual	3.25	1.10				
Cor Total	1081.312	49				

Note: Hz-Homogenization, Mw-Molecular weight, T-group- Terminal group, Adj-Adjusted, Pred-Predicted, Adeq-Adequate, Prec- Precision .

Table 5: Experimental matrix of PBD (Encapsulation efficiency

Response 3: Zeta Potential					**Fit Statistics**	
Source	**Sum of squares**	**Mean**	**F-value**	**p-value**		
Model	141.26	17.78	592.25	0.0001	Std. Dev.	0.18
PGA Cont.	1.04	1.04	57.31	0.002	Mean	6.85
PVA %	2.52	2.52	71.41	0.004	C.V. %	2.38
Hz Speed (rpm)	1.24	1.24	50.70	0.0014	R^2	0.99
Hz duration	3.76	3.76	7.7E-06	0.08404	Adjusted R^2	0.99
PVA Mw (kDa)	124.84	128.84	0.0063	0.00035	Predicted R^2	0.98
PGA T-Group	0.07	0.02	45.12	0.108626	Adeq. Prec.	63.21
Residual	44.22	14.74				

Cor Total	318.94	49

Note: Hz-Homogenization, Mw-Molecular weight, T-group- Terminal group, Adj-Adjusted, Pred-Predicted, Adeq-Adequate, Prec- Precision .

Table 6: Experimental matrix of PBD (Zeta potential).

Run	Independent variables			Dependable variables		
(NF)	Polymer Cont.	% PVA	Homogenization speed	Particle size (nm)	Encapsulation efficiency (%)	Zeta potential (mV)
1	1	0	1	242.70	70.15	-10.11
2	1	0	-1	318.28	72.42	-11.24
3	-1	-1	0	251.51	34.41	-4.23
4	0	-1	-1	292.63	61.38	-9.32
5	0	1	-1	281.28	64.6	-710
6	0	0	0	228.64	68.37	-9.31
7	1	1	0	274.21	80.29	-8.12
8	-1	0	-1	260.35	37.79	-4.32
9	0	0	0	221.3	73.15	-8.43
10	0	0	0	228.41	71.63	-8.12
11	0	0	0	230.17	71.34	-8.08
12	0	0	0	222.47	72.16	-8.04
13	-1	0	1	201.25	39.21	-4.21
14	1	-1	0	284.72	68.16	-10.43
15	-1	1	0	214.38	36.15	-4.12
16	0	1	1	205.47	61.27	-8.24
17	0	-1	1	2254.38	60.17	-9.23

Table 7: BBD of three variable systems.

Determination of particle size of NPs

The average diameter of nanoparticles (NPs) ranged from 203.24 nm to 318.20 nm across the 17 experimental runs detailed in the Box-Behnken Design (BBD) (see Table 5-5). The polynomial equation demonstrated how the independent variables (X1, X2, and X3) influenced the particle size. Notably, a positive coefficient for X1 indicated a favorable impact on particle size, while negative coefficients for X2 and X3 suggested a decrease in size. ANOVA analysis revealed that increasing the concentration of PGA was associated with a larger average particle diameter. Elevated PGA concentrations increased the viscosity of the PGA solution (NF 1), which in turn required higher shear stress to produce smaller particle sizes . If the homogenization speed is inadequate (NF 2), it may not provide sufficient shear stress, leading to larger particle diameters. During the secondary emulsification phase, the size of the primary emulsion droplets indicates the dispersion into a larger volume.

$Y1 = 226.60 + 23.81X1 - 9.86X2 - 34.72X3 + 6.65X1X2 + 17.53X1^2 + 13.07X2^2 + 12.02X3$

Particle Size					
Source	**Sum of**	**Df**	**Mean**	**F-value**	**p-value**
Model	18121.56	9	2012.40	117.21	0.00
PGA Cont. (A)	4523.42	1	4531.42	260.65	0.00

PVA (B)	779.15	1	779.15	43.91	0.00
Homogenizationspeed (C)	9632.44	1	9641.44	557.53	0.00
AB	178.16	1	178.16	11.22	0.02
AC	53.42	1	52.42	2.03	0.12
BC	19.32	1	19.32	1.06	0.33
AÂ²	1293.42	1	1293.42	73.71	0.00
BÂ²	718.65	1	718.65	41.54	0.00
CÂ²	607.19	1	607.19	35.10	0.00
Residual	122.28	7	18.33		
Lack of Fit	53.07	3	19.36	1.11	0.42
Pure Error	66.21	4	17.55		
Cor Total	36168.29	16			

Table 8: ANOVA results of encapsulation efficiency in BBD.

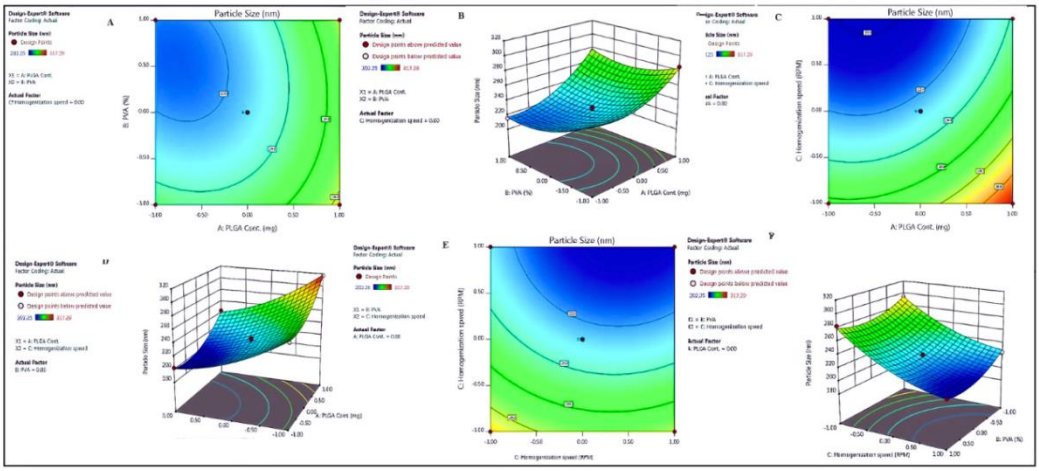

Figure 11: Contour plots and 3D response surface plots showing the effect of different variables on the particle size of levofloxacin loaded nanoparticles

Entrapment and loading efficiency measurement

The encapsulation efficiency of the nanoparticles ranged from 34.41% to 80.29% across the experimental runs outlined in. An F-value of 107.97 for the second-order response surface model demonstrates its significance at the 5% level. The model achieved a predictive R^2 value of 0.9398 and an adjusted R^2 value of 0.9834, indicating a strong level of accuracy. An adequate ratio of 28.83 confirms a solid signal, underscoring the model's effectiveness in optimizing the design space. The polynomial equation (Equation 8) illustrates that the independent variables X1 and X2 significantly influence drug encapsulation efficiency (NF 1, 8), as depicted in .The lipophilic properties of levofloxacin (22) enhance its incorporation into PGA, which reduces drug diffusion. However, the crystalline form of levofloxacin negatively affects encapsulation efficiency. Conversely, the amorphous form of the drug within the nanoparticles indicates that high encapsulation efficiency is achieved due to favorable interactions with the polymer matrix. The final model, detailed in Table 5-7, effectively fits the encapsulation efficiency data, achieving an R^2 value of 0.99 (35).

$Y2 = 71.73 + 18.66X1 + 2.54X2 + 3.10X1X2 - 11.48X1\ 2 - 5.00X2\ 2 - 4.90X32$

Encapsulation efficiency					
Source	**Sum of**	**df**	**Mean**	**F-value**	**p-value**
Model	3721.17	9	412.80	106.92	0.00
PGA Cont.(A)	2775.19	1	2775.19	720.03	0.00
PVA (B)	50.46	1	50.46	13.32	0.01
Homogenization speed (C)	6.62	1	6.62	1.71	0.22
AB	37.31	1	37.31	9.91	0.02
AC	7.53	1	7.53	1.94	0.20
BC	4.03	1	4.03	1.03	0.33
AÂ²	553.01	1	553.01	143.43	0.00
BÂ²	104.12	1	104.12	27.12	0.00
CÂ²	102.23	1	101.25	26.14	0.00

Residual	24.07	7	3.87		
Lack of Fit	11.72	3	4.24	1.13	0.40
Pure Error	14.35	4	3.59		
Cor Total	3751.25	16			

Table 9: ANOVA results of encapsulation efficiency in BBD.

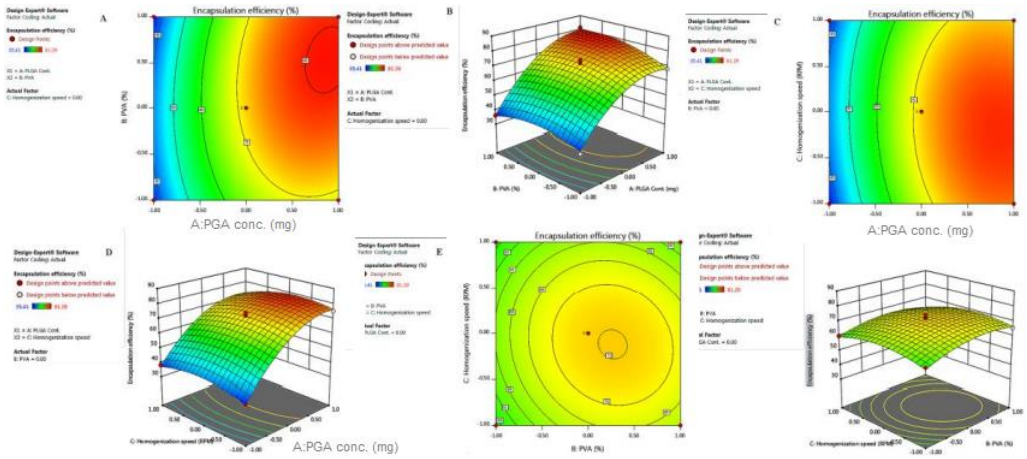

Figure 12: Contour plots and 3D response surface plots showing the effect of different variables on the encapsulation efficiency of levofloxacin loaded nanoparticles

Determination of zeta potential of NPs

In the double emulsion solvent evaporation method, zeta potential quantifies the electrical potential difference between the stationary phase of dispersed particles and the surrounding dispersion medium . This measurement is vital for assessing the stability of colloidal dispersions. Generally, higher zeta potential values are associated with greater stability, as they indicate that the repulsive forces between particles surpass any attractive forces . In contrast, emulsions exhibiting low zeta potential values are more prone to coagulation or flocculation, which can compromise physical stability (34) .

In this investigation, zeta potential values varied between –4.31 mV and –10.72 mV. The F-value of 48.08 indicates that the second-order response surface model accurately fits the experimental data, with only a 0.01% probability that such a large F-value is due to random variation. The predicted R^2 value of 0.8572 aligns closely with the adjusted R^2 value of 0.9637, reflecting a high degree of predictive reliability.

The effect of homogenization speed on zeta potential was relatively minor, with zeta potential values increasing as the stirring speed rose (NF 1, 2) . Furthermore, an inverse relationship was observed between particle size and zeta potential, with smaller particle sizes generally correlating with higher zeta potential values (23). The polynomial equation used to predict zeta potential is as follows:

$Y3 = 9.60 + 2.24X1 - 0.79X2 + 0.40X3 - 1.04X1X2 - 1.34X1\ 2 - 1.5X2$

Zeta Potential					
Source	**Sum of**	**df**	**Mean**	**F-value**	**p-value**
Model	68.91	9	7.72	47.08	0.00
PGA Cont. (A)	40.12	1	40.12	249.45	0.00
PVA (B)	5.07	1	5.07	30.29	0.00
Homogenizationspeed (C)	1.31	1	1.31	8.01	0.03
AB	4.32	1	4.32	26.72	0.00
AC	0.03	1	0.03	0.24	0.60
BC	0.63	1	0.63	4.07	0.08
AÂ²	7.58	1	7.58	44.00	0.00
BÂ²	9.40	1	9.40	59.48	0.00
CÂ²	0.11	1	0.11	0.60	0.42
Residual	1.11	7	0.16		
Lack of Fit	0.53	3	0.19	1.40	0.38
Pure Error	0.54	4	0.14		
Cor Total	71.04	16			

Table 10: ANOVA results of Zeta potential in BBD.

6.4.3 Desirability and Validation of the Statistical Model

The optimization of the nanoparticle (NP) formulation was guided by desirability criteria and an overlay plot generated using Design-Expert software . A desirability score of 0.884 indicates a high degree of accuracy in meeting the desired formulation characteristics. To confirm the validity of the optimized formulation, experimental results for Levofloxacin-PGA-NPs were compared to these predicted values. The results showed less than a 10% deviation between the experimental data for particle size, encapsulation efficiency, and zeta potential compared to the predicted values. The final formulation achieved a drug loading of 76.31%, as derived from the optimization process using Design-Expert Software. A comprehensive summary of the predicted and experimental data for the optimization of Levofloxacin-PGA-NPs is presented.

Chromatographic Conditions

The quantitative determination of levofloxacin concerning solubility and pharmacokinetic analysis was conducted using validated LC-MS/MS methods for both analytical and bioanalytical assessments. A single set of LC optimized parameters was used for all quantification studies. Effective chromatographic separation of the drug from matrices was achieved using a reverse-phase C18 column with an appropriately programmed gradient mobile phase (24). The binary HPLC system utilized a combination of acetonitrile (Pump B) and water (Pump A) to facilitate gradient flow, allowing plasma to elute first, followed by LEV for optimal response. The LC system's flow rate was fixed at 0.3 ml/min (with a maximum allowable flow of 0.5 ml/min for the API2000 MS/MS) to ensure reproducibility. The autosampler temperature was maintained at 15°C, and the injection volume was set to 15 µl, while no temperature was applied in the column oven. The optimized LC parameters for both methods are summarized.

Name	Goal	Lower	Upper	Importance	Predicted value	Experimental value	Bias (%)
PGA Cont.	is in range	-1	1	3	0.438		
PVA%	is in range	-1	1	3	0.011		
Homogenization speed	is in range	-1	1	3	0.728		
Particle Size	minimize	201.25	314.29	3	221.03	231.4	-5.60
Encapsulation efficiency	maximize	34.41	80.29	3	73.97	78.21	-7.08
ZetaPotential	maximize	4.31	11.73	3	10.54	9.90	5.97

Table 11: Comparison of the predicted and experimental values of the Response Variables of LEV-PGA-NPs.

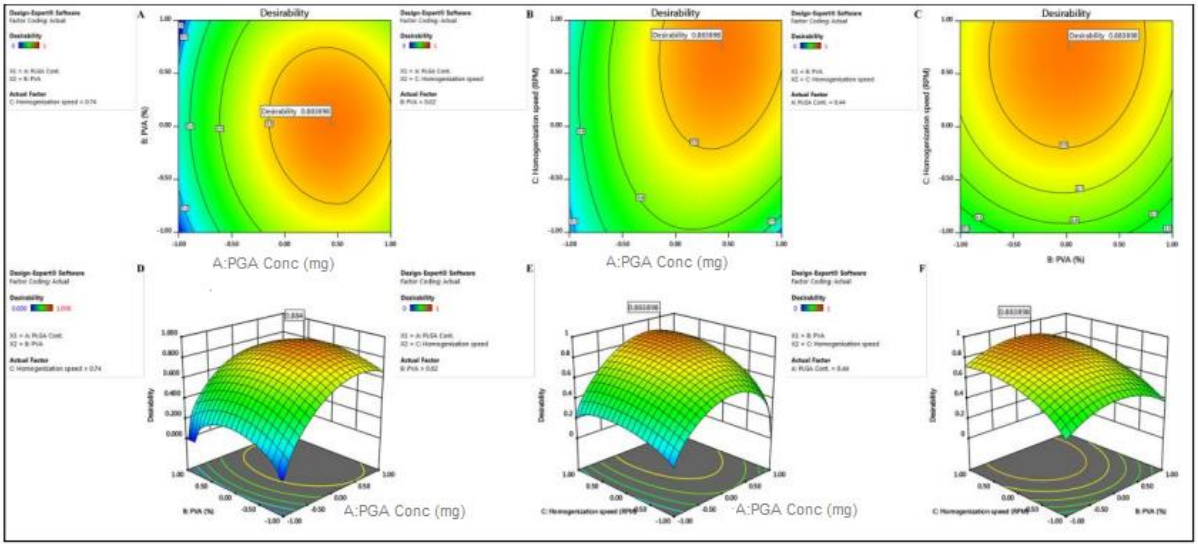

Figure 13: Contour and 3D representation of optimization graph with disability score.

Evaluation of optimized nanoparticles

The properties and functionality of the optimized nanoparticles were validated through various evaluation techniques. Key characteristics, such as nanoparticle size, surface energy, morphological analysis, and physicochemical stability of both the drug and excipients, were assessed prior to their application in rodent models.

Determination of Surface Morphology, Particle Size, and Zeta Potential

The scanning electron microscopy (SEM) images were analyzed to provide insights into the morphology, particle size, and aggregation behavior of the optimized nanoparticles, as illustrated. SEM micrographs taken at various magnifications revealed that the levofloxacin loaded nanoparticles exhibited a nearly monodispersed spherical shape without any visible signs of aggregation. The smooth surface of the nanoparticles is likely to facilitate a uniform sustained release of the drug. Particle size and zeta potential data for the optimized nanoparticles are presented, with a detailed discussion on these parameters found in the statistical optimization section (25).

Physicochemical Stability

FTIR Study

The compatibility of the drug with the excipients was evaluated using Fourier-transform infrared (FTIR) spectroscopy on both the physical mixture and the drug-loaded nanoparticles. The FTIR spectra for levofloxacin, PGA and the physical mixture of levofloxacin -PLGA were previously reported in the preformulation study. In this section, the physicochemical integrity of each component of the optimized nanoparticles was assessed using FTIR across a range of 3600 cm^{-1} to 400 cm^{-1}.. The FTIR spectra of the optimized levofloxacin -PGA nanoparticles exhibited characteristic peaks corresponding to pure levofloxacin: 3062.14 cm^{-1} (aromatic C-H stretching from benzene rings), 2960.44 cm^{-1} (aliphatic C-H bond stretching), 1693.20 cm^{-1} (carbonyl C=O group of carboxylic acid), 1450.98 cm^{-1} (C=C aromatic group), and 749.85 cm^{-1} (ring vibration of 1,2-disubstituted benzene). Additionally, PGA peaks were identified at 1757.28 cm^{-1} (C=O stretching of the carbonyl group), 1454.40 cm^{-1} (C-H stretching from methyl groups), and 1190.29 cm^{-1} and 1091.94 cm^{-1} (C-O stretching vibrations). No significant shifts in the characteristic peaks of the drug and excipients were observed, indicating a lack of major chemical interactions between them. Overall, the findings confirm the chemical integrity of the drug dispersed within the polymeric nanoparticles.

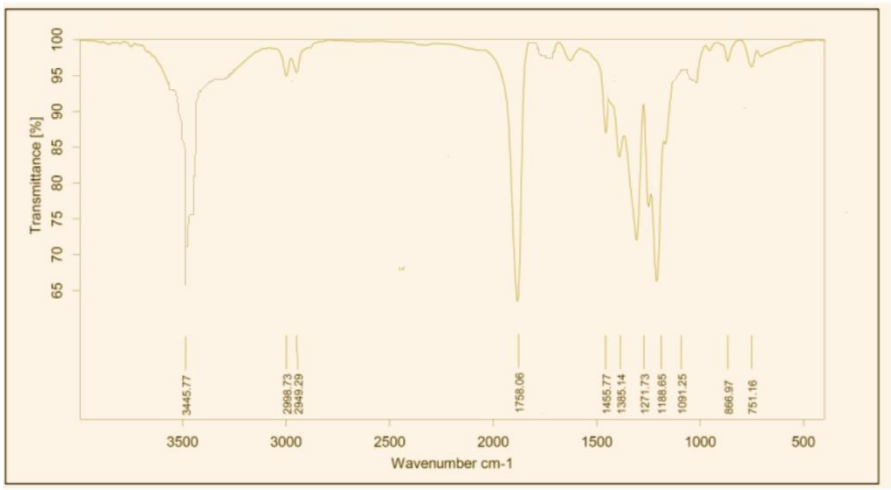

Figure 14: Fourier-transform infrared (FT-IR) spectra of Levofloxacin loaded NPs

DSC, XRD and MS/MS study

The physical properties of both the active pharmaceutical ingredient (API) and the polymer play a crucial role in determining the therapeutic application of the drug. The physical states of the drug and polymer within nanoparticles (NPs) were characterized to evaluate the functionality of the formulation. In this context, the drug can exist in various forms, such as crystalline or amorphous, when coexisting with the polymer. During the formulation process, different solvents and surfactants were introduced alongside the drug and polymer. To assess any potential unwanted interactions between the drug and polymer, differential scanning calorimetry (DSC), X-ray diffraction (XRD), and mass spectrometry (MS/MS) analyses were conducted. The thermal profile of the optimized levofloxacin -PGA-NPs was compared to the individual thermal graphs of the polymer, the drug, and the previously analyzed levofloxacin -PGA physical mixtures .. Notably, the thermogram for the levofloxacin -PGA-NPs did not exhibit the characteristic melting peak of levofloxacin at 271.30°C. Crystallinity, which can influence the drug release characteristics from NPs, was also analyzed using XRD. The diffractogram of levofloxacin -PGA-NPs presented a more uniform baseline, supporting the amorphous nature of the formulation. The characteristic peaks of TLM at 6.8°, 14.2°, 15.1°, and 22.3° were absent in the diffractogram of levofloxacin -PGA-NPs. This loss of intense peaks at those diffraction angles suggests that levofloxacin may have transitioned into an amorphous solid dispersion.

Further analysis of levofloxacin was conducted using LC-MS/MS before and after NP preparation. The +Q1 and MS2 scans confirmed the transition pairs (M+H+) m/z 514.2→274.2 for levofloxacin and 610.2→422.2 for the internal standard, candesartan cilexetil (CAN).

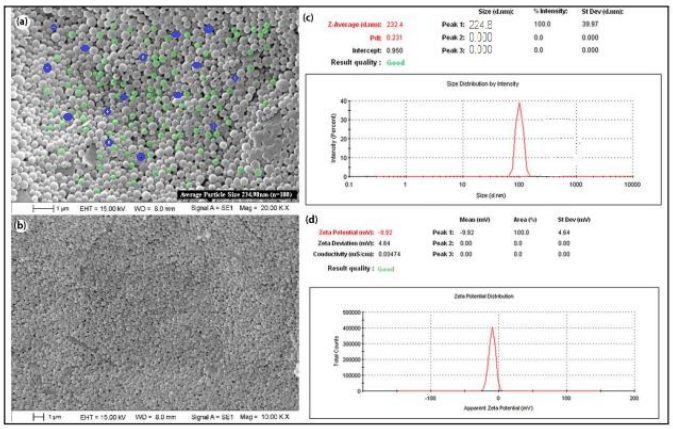

Figure 15: SEM images of Levofloxacin -PGA-NPs-07 (a) magnification at 20KX (b) magnification at 10KX and (c) particle size distributions and (d) zeta potential

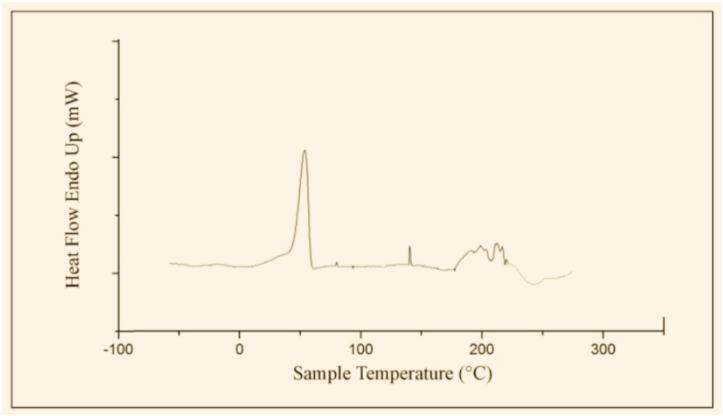

Figure 16: DSC thermograms of Levofloxacin loaded PGA nanoparticles.

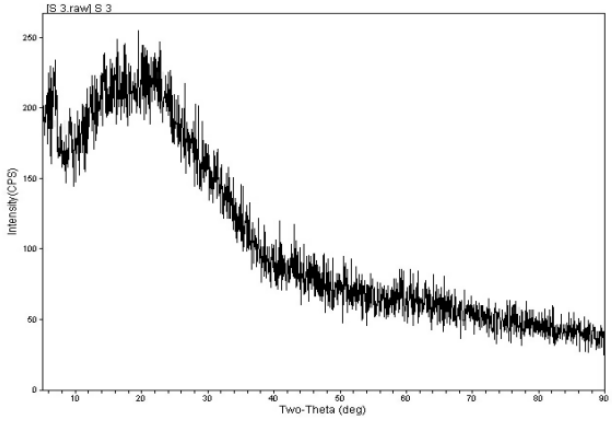

Figure 17: XRD studies of Levofloxacin loaded PGA nanoparticles

Encapsulation efficiency

The double emulsion solvent evaporation technique offers significant benefits for formulating nanoparticles (NPs) with both hydrophilic and lipophilic active pharmaceutical ingredients (APIs). X-ray diffraction (XRD) analysis revealed characteristic peaks for pure levofloxacin at 14.3°, 15.04°, 18.34°, 22.34°, and 25.04° which were compared to those of the LEV-loaded NPs (Figure 5-26). The degree of crystallinity was calculated, and among all formulations, formulation-7 exhibited the highest encapsulation efficiency while showing no detectable crystalline Levofloxacin (27).The optimized formulation achieved an impressive encapsulation efficiency of 79.21%, and characterization results indicate a uniform solid dispersion of Levofloxacin within the polymer matrix.

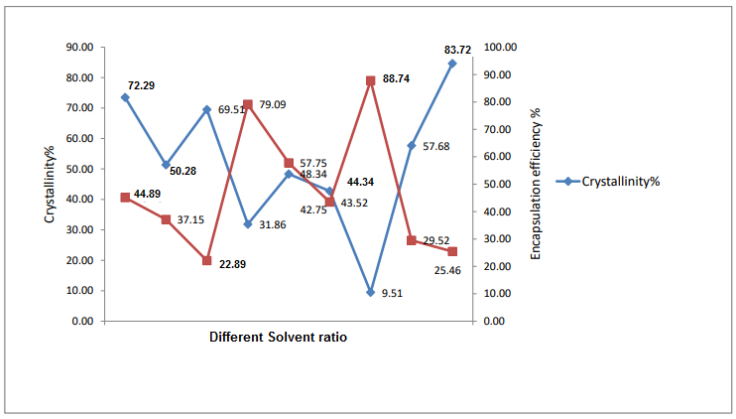

Figure 18: Comparative representation of crystallinity and encapsulation efficiency

Drug Loading

Assessing drug loading in nanoparticles (NPs) is analogous to determining encapsulation efficiency, as both require measuring the drug content within the NPs. Drug loading reflects the ability of NPs to retain drug molecules within the polymer matrix. In this study, NPs were prepared using the double emulsification method, which facilitated the entrapment of drugs in the oil phase of the polymer matrix. The optimized formulation, designated as formulation-7, achieved a high loading value, with a quantification study indicating a drug loading of 76.30%.

In Vitro Drug Release Study

A key feature of polymeric NPs is their ability to provide a sustained release profile, as highlighted by Hirenkumar K. Makadia et al. In this study, poly(lactic-co-glycolic acid) (PGA) was utilized to formulate the polymeric NPs. PGA degrades via hydrolysis of its ester linkages when exposed to water, and previous research suggests that PGA (50:50) has a degradation period of up to 102 days. Consequently, a prolonged release profile over 384 hours was observed for the LEV-PGA-NPs in phosphate-buffered saline (PBS) at pH 7.4.(30)

To assess therapeutic efficacy, the release patterns of LEV tablets (250 mg) and LEV -PGA-NPs were compared .The curve-fitting data for the in vitro release kinetics are summarized, showing high regression coefficients. Among the models tested, the Korsmeyer–Peppas model (R^2=0.924) provided the best fit, outperforming the zero-order, first-order, and Higuchi models (28). The release data for the optimized formulation conformed to the Korsmeyer–Peppas equation, indicating that LEV-PGA-NPs followed Fickian diffusion (n=0.434). These findings suggest that LEV release from the polymeric NPs occurred via a controlled diffusion mechanism.

Model	R^2	Release exponent (n)
Korsmeyer–Peppas	0.924	0.434
Higuchi	0.902	-
Zero order	0.694	-
First order	0.431	-

Table 10: Results of curve fitting of the in vitro release of LEV from the optimized formulation

Antimicrobial activity

In this study, the antimicrobial efficacy of synthesized Lev/Mox nanoparticles (Lev/Mox-NPs) was evaluated against three species of highly pathogenic, multidrug-resistant bacteria (31). The antimicrobial activity of Lev/Mox-NPs was compared to conventional antibacterial agents such as doxycycline and ciprofloxacin. The average particle size of the nanoparticles used in the study. The synthesized Lev/Mox nanoparticles (NPs) demonstrated antimicrobial activity against all tested microorganisms (32).The result shows below.

Tested strains	Doxycycline (Standard antibacterial agent)	Ciprofloxacin (Standard antibacterial agent agent)	Diameter of inhibition zone. (mm) produced by AgNPs	P-value	
Std. Agent Dose 500 mg			B Mean ± SD	A Mean ± SD	Xxxxxxxxxx
Brucella melitensis	24	-	27.67± 0.577 LEV	22.67±1.155 LEV	0.0131●
			28.37± 0.543 MOX	21.87±1.175 MOX	0.0134●
Brucella	28	-	37.00± 2.646	31.33±1.155	0.0422●

melitensis A			LEV 39.00± 1.439 MOX	LEV 30.43±1.125 MOX	 0.0732
Brucella melitensis B	30	-	28.67± 1.155 LEV	34.33± 3.055 LEV	0.0848
			23.29± 1.148 MOX	38.23± 3.021 MOX	0.0328●

* Three repeats were performed for each tested strain
B: Before in-vitro gamma-irradiation.
A : After in-vitro gamma-irradiation
●P- value significant < 0.05 P- value non-significant > 0.05

Table 11: The antimicrobial activity (inhibition zone in mm) of the AgNPs synthesized against different strains before and after in –vitro gamma irradiation

Tested strains	MIC (µg/ml)		MIC50 (µg/ ml)		MIC90 (µg/ ml)		MLC(µg/ml)	
	B	A	B	A	B	A	B	A
Brucella melitensis	200	200	50	50	100	100	400	400
Brucella melitensis A	200	100	50	50	100	100	200	200
Brucella melitensis B	400	400	100	200	200	400	800	800

* Three repeats were performed for each tested strain
B: Before in-vitro gamma-irradiation.
A : After in-vitro gamma-irradiation

Table 12: Minimum inhibitory and minimum lethal concentration values of the LEV/MOX NPs synthesized for the selected strain

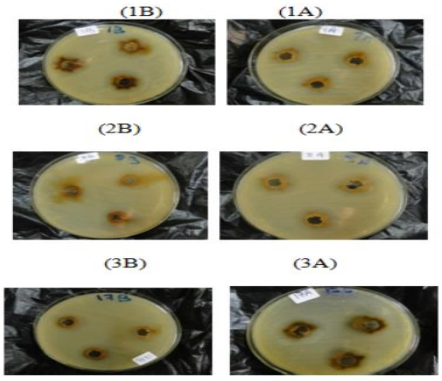

Figure 19: Representative photographs showing antimicrobial activity of the synthesized snanoparticles against *Brucella melitensis* , according to the agar well diffusion method.

REFERENCES

1. Acha, P. N., & Szyfres, B. (2001). *Zoonoses and communicable diseases common to man and animals* (3rd ed.). Pan American Health Organization.
2. Araj, G. F. (2010). Update on laboratory diagnosis of human brucellosis. *International Journal of Antimicrobial Agents*, *36*(S1), S12-S17. https://doi.org/10.1016/j.ijantimicag.2010.06.014
3. Atluri, V. L., Xavier, M. N., de Jong, M. F., den Hartigh, A. B., & Tsolis, R. M. (2011). Interactions of *Brucella* spp. with the immune system. *Nature Reviews Microbiology*, *9*(12), 811-820. https://doi.org/10.1038/nrmicro2655
4. Barbier, T., Nicolas, C., & Letesson, J. J. (2011). Brucella adaptation and survival at the crossroad of metabolism and virulence. *FEBS Letters*, *585*(19), 2929-2934. https://doi.org/10.1016/j.febslet.2011.08.046
5. Boschiroli, M. L., Foulongne, V., & O'Callaghan, D. (2001). Brucellosis: A worldwide zoonosis. *Current Opinion in Microbiology*, *4*(1), 58-64. https://doi.org/10.1016/S1369-5274(00)00165-X

6. Camacho-Sanchez, M., Díaz-Hernández, F., & Rodríguez-Morales, A. J. (2020). Human brucellosis: Update on treatment. *Infectious Disorders - Drug Targets, 20*(2), 87-97. https://doi.org/10.2174/1871526520666200107121846
7. Corbel, M. J. (2006). Brucellosis in humans and animals. *World Health Organization*.
8. Cutler, S. J., Whatmore, A. M., & Commander, N. J. (2005). Brucellosis – new aspects of an old disease. *Journal of Applied Microbiology, 98*(6), 1270-1281. https://doi.org/10.1111/j.1365-2672.2005.02622.x
9. Dadar, M., Tiwari, R., Sharun, K., Dhama, K., & Iqbal, Y. (2021). Overview of challenges and advancements in the treatment of brucellosis. *Infection and Drug Resistance, 14*, 415-429. https://doi.org/10.2147/IDR.S272251
10. El-Sayed, A., & Awad, W. F. (2018). Brucellosis: Evolution and expansion of a global challenge. *Journal of Biological Research-Thessaloniki, 25*(1), 1-10. https://doi.org/10.1186/s40709-018-0083-6
11. Franco, M. P., Mulder, M., Gilman, R. H., & Smits, H. L. (2007). Human brucellosis. *The Lancet Infectious Diseases, 7*(12), 775-786. https://doi.org/10.1016/S1473-3099(07)70286-4
12. Godfroid, J., Scholz, H. C., Barbier, T., Nicolas, C., Wattiau, P., & Fretin, D. (2011). Brucellosis at the animal/ecosystem/human interface at the beginning of the 21st century. *Preventive Veterinary Medicine, 102*(2), 118-131. https://doi.org/10.1016/j.prevetmed.2011.04.007
13. Gorvel, J. P., & Moreno, E. (2002). Brucella intracellular life: From invasion to intracellular replication. *Veterinary Microbiology, 90*(1-4), 281-297. https://doi.org/10.1016/S0378-1135(02)00214-6
14. Grilló, M. J., Blasco, J. M., Gorvel, J. P., Moriyón, I., & Moreno, E. (2012). What have we learned from brucellosis in the mouse model? *Veterinary Research, 43*(1), 29. https://doi.org/10.1186/1297-9716-43-29
15. Kaur, T., & Rana, V. (2018). Nanotechnology-based targeted drug delivery for the treatment of brucellosis: A review. *Journal of Drug Delivery Science and Technology, 44*, 127-134. https://doi.org/10.1016/j.jddst.2017.12.014
16. Ko, J., & Splitter, G. A. (2003). Molecular host-pathogen interaction in brucellosis: Current understanding and future approaches to vaccine development for mice and humans. *Clinical Microbiology Reviews, 16*(1), 65-78. https://doi.org/10.1128/CMR.16.1.65-78.2003
17. Krassakopoulou, A., & Karatapanis, S. (2021). Management of human brucellosis: An update. *Journal of Infection and Public Health, 14*(2), 205-216. https://doi.org/10.1016/j.jiph.2020.11.002
18. Lei, S., Dong, Q., Luo, Y., Wang, Y., & Qin, J. (2016). Advances in nanomedicine for the treatment of brucellosis. *Advanced Drug Delivery Reviews, 106*, 46-58. https://doi.org/10.1016/j.addr.2016.06.008
19. López-Santiago, R., Sánchez-García, F. L., & Carranza, C. (2020). Brucellosis diagnosis: An update. *Open Veterinary Journal, 10*(1), 1-9. https://doi.org/10.4314/ovj.v10i1.1
20. Memish, Z. A., & Balkhy, H. H. (2004). Brucellosis and international travel. *Journal of Travel Medicine, 11*(1), 49-55. https://doi.org/10.2310/7060.2004.13661
21. Moreno, E. (2014). Retrospective and prospective perspectives on zoonotic brucellosis. *Frontiers in Microbiology, 5*, 213. https://doi.org/10.3389/fmicb.2014.00213
22. Moriyon, I., Grillo, M. J., Monreal, D., Gonzalez, D., Marin, C. M., & Lopez-Goni, I. (2004). Rough vaccines in animal brucellosis: Structural and genetic basis and present status. *Veterinary Research, 35*(1), 1-38. https://doi.org/10.1051/vetres:2003048
23. Navidpour, L., & Emadi, M. (2017). Nanotechnology-based drug delivery systems for targeting 23. intracellular *Brucella*. *International Journal of Nanomedicine, 12*, 5433-5452. https://doi.org/10.2147/IJN.S140509
24. Pappas, G., Akritidis, N., Bosilkovski, M., & Tsianos, E. (2005). Brucellosis. *The New England Journal of Medicine, 352*(22), 2325-2336. https://doi.org/10.1056/NEJMra050570
25. Pappas, G., Papadimitriou, P., Akritidis, N., Christou, L., & Tsianos, E. V. (2006). The new global map of human brucellosis. *The Lancet Infectious Diseases, 6*(2), 91-99. https://doi.org/10.1016/S1473-3099(06)70382-6
26. Rajashekara, G., Glasner, J. D., Glover, D. A., & Splitter, G. A. (2004). Comparative whole-genome hybridization reveals genomic islands in *Brucella* species. *Journal of Bacteriology, 186*(15), 5040-5051. https://doi.org/10.1128/JB.186.15.5040-5051.2004
27. Seleem, M. N., Boyle, S. M., & Sriranganathan, N. (2010). Brucellosis: A re-emerging zoonosis. *Veterinary Microbiology, 140*(3-4), 392-398. https://doi.org/10.1016/j.vetmic.2009.06.021
28. Shafiei, R., Owlia, P., & Jalali-Nadoushan, M. R. (2021). Advances in nanotechnology-based approaches for drug delivery in brucellosis therapy. *International Journal of Nanomedicine, 16*, 2063-2080. https://doi.org/10.2147/IJN.S298102
29. Tian, Z., Zhang, Y., Chen, D., & Xu, S. (2019). Current strategies for the treatment of brucellosis and targeted drug delivery. *Pharmacology & Therapeutics, 195*, 1-9. https://doi.org/10.1016/j.pharmthera.2019.10.007
30. Young, E. J. (1995). An overview of human brucellosis. *Clinical Infectious Diseases, 21*(2), 283-289. https://doi.org/10.1093/clinids/21.2.283
31. Almeida, B., Souto, E. B., & Silva, A. M. (2015). Solid lipid nanoparticles as a drug delivery system for peptides and proteins. *Advanced Drug Delivery Reviews, 106*, 259-274. https://doi.org/10.1016/j.addr.2015.07.021
32. 32. Anselmo, A. C., & Mitragotri, S. (2019). Nanoparticles in the clinic: An update. *Bioengineering & Translational Medicine, 4*(3), e10143. https://doi.org/10.1002/btm2.10143
33. 33. AshaRani, P. V., Low Kah Mun, G., Hande, M. P., & Valiyaveettil, S. (2009). Cytotoxicity and genotoxicity of silver nanoparticles in human cells. *ACS Nano, 3*(2), 279-290. https://doi.org/10.1021/nn800596w

34. 34. Bazak, R., Houri, M., El Achy, S., Kamel, S., & Refaat, T. (2015). Cancer active targeting by nanoparticles: A comprehensive review of literature. *Journal of Cancer Research and Clinical Oncology, 141*(5), 769-784. https://doi.org/10.1007/s00432-014-1767-3
35. 35 Carbone, C., Campisi, A., Musumeci, T., & Puglisi, G. (2015). Nanomaterials for enhancing the oral bioavailability of poorly water-soluble drugs. *Current Pharmaceutical Design, 21*(19), 2512-2525. https://doi.org/10.2174/1381612821666150311161855
36. 36. Cho, K., Wang, X., Nie, S., Chen, Z., & Shin, D. M. (2008). Therapeutic nanoparticles for drug delivery in cancer. *Clinical Cancer Research, 14*(5), 1310-1316. https://doi.org/10.1158/1078-0432.CCR-07-1441